Bioinspiration & Biomimetics

PAPER

The effect of wing flexibility on sound generation of flapping wings

To cite this article: Biao Geng *et al* 2018 *Bioinspir. Biomim.* **13** 016010

Manuscript version: Accepted Manuscript

Accepted Manuscript is "the version of the article accepted for publication including all changes made as a result of the peer review process, and which may also include the addition to the article by IOP Publishing of a header, an article ID, a cover sheet and/or an 'Accepted Manuscript' watermark, but excluding any other editing, typesetting or other changes made by IOP Publishing and/or its licensors"

This Accepted Manuscript is© .

During the embargo period (the 12 month period from the publication of the Version of Record of this article), the Accepted Manuscript is fully protected by copyright and cannot be reused or reposted elsewhere.

As the Version of Record of this article is going to be / has been published on a subscription basis, this Accepted Manuscript will be available for reuse under a CC BY-NC-ND 3.0 licence after the 12 month embargo period.

After the embargo period, everyone is permitted to use copy and redistribute this article for non-commercial purposes only, provided that they adhere to all the terms of the licence https://creativecommons.org/licences/by-nc-nd/3.0

Although reasonable endeavours have been taken to obtain all necessary permissions from third parties to include their copyrighted content within this article, their full citation and copyright line may not be present in this Accepted Manuscript version. Before using any content from this article, please refer to the Version of Record on IOPscience once published for full citation and copyright details, as permissions may be required. All third party content is fully copyright protected, unless specifically stated otherwise in the figure caption in the Version of Record.

View the article online for updates and enhancements.

This content was downloaded from IP address 18.119.131.72 on 05/05/2024 at 05:39

THE EFFECT OF WING FLEXIBILITY ON SOUND GENERATION OF FLAPPING WINGS

Biao Geng, Qian Xue and Xudong Zheng
Department of Mechanical Engineering
University of Maine
Orono, ME, USA

Geng Liu, Yan Ren and Haibo Dong
Department of Mechanical and Aerospace Engineering
University of Virginia
Charlottesville, VA, USA

ABSTRACT

In this study, the unsteady flow and acoustic characteristics of a three-dimensional (3D) flapping wing model of Tibicen linnei cicada at forward flight condition are numerically investigated. A single cicada wing is modelled as a membrane with prescribed motion reconstructed from high-speed videos of a live insect. The numerical solution takes a hydrodynamic/acoustic splitting approach: the flow field is solved with an incompressible Navier-Stokes flow solver based on immersed boundary method and the acoustic field is solved with linearized perturbed compressible equations (LPCEs). The 3D simulation allows examination of both directivity and frequency composition of the flapping wing sound in the full space. Along with the flexible wing model, a rigid wing model that is extracted from the real motion is also simulated to investigate the effect of wing flexibility.

The simulation results show that the flapping sound is directional; the dominant frequency varies around the wing. The first and second frequency harmonics show different radiation patterns in the rigid and flexible wing cases which are demonstrated to be highly associated with wing kinematics and loadings. Furthermore, the rotation and deformation in the flexible wing is found to help lower the sound strength in all the directions.

Introduction

The high performance and great agility of flapping-wing flight of insects have long been of interest to biologists, physicists, and engineers. Many studies have investigated the high-lift mechanism of insect flight [1,2]. The aerodynamic sound of flying insects, on the contrary, has received less attention [3,4]. Nevertheless, it's worth noticing that the high-lift performance of insect flight is achieved with low noises, which might be important in some biomimetic applications, such as ultra-quiet micro air vehicles. Besides, the flapping sound could also bear important biological functions such as sexual communication [5] and perhaps sending aposematic signals [6], in which cases the locomotion-induced sounds that have evolved specially for communication are termed sonations [7]. In the study by Robert and Göpfert [8], it was shown that the antennae of several higher fly representatives responded to the sound physically similar to their own species, which adds proof to that the flapping sound could be sonation rather than the incidental noise of locomotion. But can insects actively control their acoustic message during flight maneuver? Or is it just the involuntary sound that's utilized as it is? Could the sound be directed to intended receivers?

To answer questions like these, one necessary step is to understand the characteristics as well as the generating mechanism of flapping sound. Sueur et al. [3] experimentally studied the radiation pattern and frequency composition of the sound of tethered flight of flies in the horizontal plane. The flapping sound was found to be directional with the wing beat frequency dominating the front and the second harmonic dominating the two sides. Bae and Moon [4] numerically investigated the flapping sound of a two-dimensional simplified rigid wing of bumblebee using a linearized perturbed compressible equations based hydrodynamic/acoustic splitting method. Their results suggested that the directivity of the flapping sound varies under different flight conditions: wing beat frequency were found to be dominant in the front and back while the second harmonic dominated in the upside and downside in hovering flight; but such pattern was not observed in the forward flight. Inada et al. [9] studied the sound radiation around the insects of different wing sizes in 3D using the Ffowcs-Williams and Hawkings method. They found that the frequency composition of the flapping sound varied around the insect and this variation was closely related to the pressure variation on the wing surfaces.

One remarkable feature in insect flight is the flexibility of the wing structure. Many studies have been conducted to answer the question whether it's a beneficial feature optimized through evolution or it's a limitation due to the finite stiffness of biological material. Young et al. [10] showed that the fully-flexible wing achieved greater power economy than the model without camber, which performed better than the model without both camber and spanwise twist. Ren and Dong [11] decomposed the wing kinematics into basic modes using single value decomposition and studied the performance of different mode

combinations. The results showed that the morphing mode accounts for about 90% of the lift production and lift economy. However, excessive flexibility in the chord-wise [12] or spanwise [13] direction were also shown to degrade aerodynamic performance. Aeroacoustics wise, the effect of wing flexibility on flapping sound production was rarely studied. One prominent difference between the rigid and flexible wings is the direction of the net force vector which follows the surface normal as the wing undergoes deformations [14]. According to Inada et al. [9], such difference in loading would also lead to a difference in the directivities of the flight sound. However, is the wing flexibility a key feature for achieving the ultra-silent flight of some insects? If so, is there an optimal flexibility for achieving both high lift and low noise? How does the wing flexibility change the sound direction? The knowledge to answer these questions is very limited.

The objective of this study is to: (a) numerically investigate the radiation pattern of the flapping sound in 3D; (b) study the effects of wing flexibility on sound directivity and level by generating a rigid wing model and flexible wing model; and (c) study the relationship between sound directivity and dynamic wing surface loading. In the study, the flapping wing is modelled as a membrane with prescribed motion reconstructed from high-speed videos of a live insect. The information gathered would help gain insight into the fundamental mechanism of the flapping sound generation.

Method

Computational methodology

This study takes a hydrodynamic/acoustic splitting approach to solve the flow and acoustic field. The flow field is modeled by the incompressible Navier–Stokes (INS) equations:

$$\nabla \cdot \vec{U} = 0$$
$$\frac{\partial \vec{U}}{\partial t} + \vec{U} \cdot \nabla \vec{U} = -\frac{1}{\rho_0} \nabla p + \nu_0 \nabla^2 \vec{U} \qquad (1)$$

where $\vec{U}, \rho_0, p, \nu_0$ are the incompressible flow velocity, density, pressure and kinematic viscosity, respectively. The INS equations are solved with our previous immersed-boundary method based flow solver [15,16].

A hydrodynamic/acoustics splitting method based acoustics solver was integrated to solve the acoustic field [17,18], which is modeled by the linearized perturbed compressible equations (LPCEs):

$$\frac{\partial \rho'}{\partial t} + \vec{U} \cdot \nabla \rho' + \rho_0 \left(\nabla \cdot \vec{u}' \right) = 0$$
$$\frac{\partial \vec{u}'}{\partial t} + \nabla \left(\vec{u}' \cdot \vec{U} \right) + \frac{1}{\rho_0} \nabla p' = 0 \qquad (2)$$
$$\frac{\partial p'}{\partial t} + \vec{U} \cdot \nabla p' + \gamma P \left(\nabla \cdot \vec{u}' \right) + \vec{u}' \cdot \nabla P = -\frac{DP}{Dt}$$

where $\rho', \vec{u}', p'$ are the acoustic perturbed flow density, velocity, and pressure, respectively, and γ is the ratio of the specific heats. The DP/Dt term represents the sound source from the flow solver. The LPCE equation is discretized with a sixth-order central compact finite difference scheme in space and integrated using a four-stage Runge-Kutta (RK4) method in time. To resolve the moving geometry of the cicada wing, a sharp-interface method based on the ghost-cell approach is employed for boundary treatment. With this splitting method, the total velocity/pressure of the flow would be the sum of the incompressible flow velocity/pressure and acoustic velocity/pressure perturbation.

The current splitting method is intended for low-Mach (Ma<0.3) flows and has been verified and tested on canonical problems of flow-induced sound with Reynolds number ranging from 100 to 10000 [17, 18]. Further details of this model can be found in the work by Seo and Mittal [18].

Wing models and simulation setup

The study employs a cicada wing model with a prescribed flexible motion which was reconstructed from high speed photogrammetry by Liu et al. [19]. A snapshot of the high-speed video of a cicada forward flight is shown in Figure 1a. The reconstruction method of the 3D flexible flapping wing kinematics can be found in Koehler et al. [20]. Similar computational models have been used in the aerodynamic studies of the cicada forward flight [19,21], where more details about the wing morphology and kinematics measurements can be found. Since the kinematics of the left and right wings are symmetric, instead of the whole cicada model, only the right wing is used in this study, which would reduce the complexity of the model and allow us to focus on the very basic mechanism of sound generation. The wing kinematics are briefly summarized here. Figure 1(b) and 1(c) shows the wing position at the beginning of the down- and upstroke in the lateral view and the view perpendicular to the mean stroke plane, respectively. The angle between the stroke plane (mean) and the horizontal plane (the x-z plane) is 36°. The stroke amplitude Φ is about 114° with the stroke angle ϕ (measured from the sagittal plane, i.e. the x-y plane) ranging from 22° to 136°. The mid-span chord length (c) is 19.6mm, and the wing span is 35mm. The flapping frequency (f) is about 46.5Hz. **The forward flight speed is 2.67m/s. The Reynolds number is about 3500 based on the chord length and the forward flight speed, and**

about 16500 based on the maximum wingtip velocity, which is about 12m/s (corresponding Mach number < 0.04).

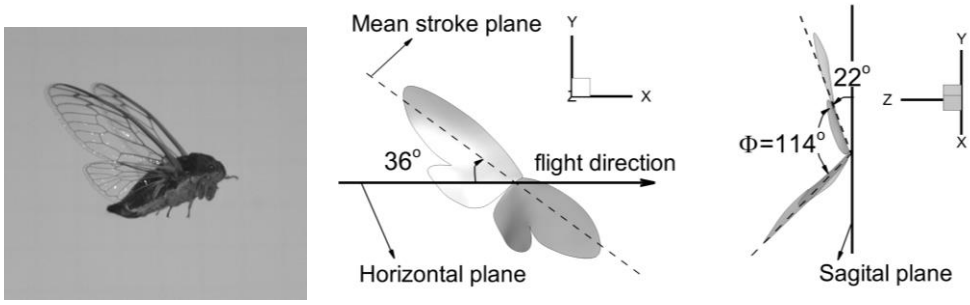

(a) (b) (c)

Figure 1. (a) A snapshot of the cicada forward flight. Wing position at the beginning of the down- and upstroke in the (b) right view and (c) view perpendicular to the mean stroke plane.

In addition to the real flexible wing model, a flapping rigid wing model was extracted from the flexible wing kinematics using a single value decomposition (SVD) method, which is a robust mathematical method for obtaining low-dimensional approximate descriptions (SVD modes) of the motion of the flexible wing model. The details of the SVD method used in this work can be found in [11], The most dominant mode (flapping mode) among all the SVD modes, which contains about 85% **of the total kinetic energy** of the flexible wing motion, is used for the rigid wing study in comparison to the computational analysis of the flexible wing model. This flapping mode rotates about the long axis of the cicada body and has no twisting about the span axis of the wing. Figure 2 shows the trajectories of the flexible and rigid wing models in the downstroke and upstroke, respectively. Compared to the flexible wing model, the rigid wing model has the same basic kinematic parameters, i.e. the same mean stroke plane and stroke angle. The difference is that the morphing mode is absent. The wing doesn't twist and remains almost perpendicular to the mean stroke plane during the entire stroke cycle. The cicada would surely not be able to fly forward with this wing kinematics. Nevertheless, it serves as a good model for the comparative study.

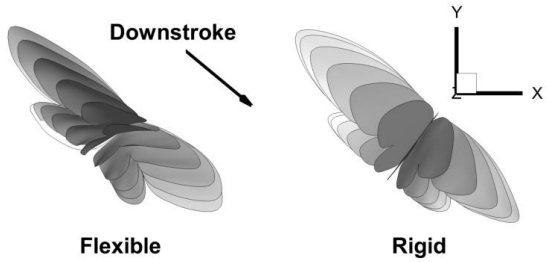

(a) Downstroke

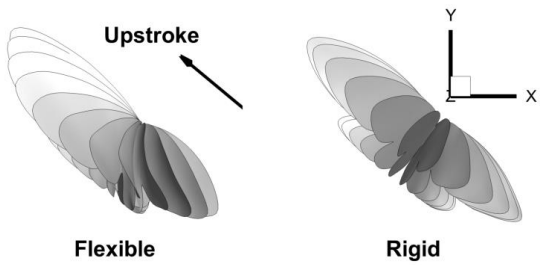

(b) Upstroke

Figure 2. Wing trajectory for the flexible model and rigid model during downstroke and upstroke.

The computational domain, as is shown in Figure 3, is a cube with a side length of $200c$. **Since resolving the flow requires much finer grid than resolving the sound wave, grid-independent studies were performed by comparing the wing drag and lift histories. The final gird used in this study is** a non-uniform Cartesian grid with $257\times257\times257$ grid points. At the center of the domain, a cubic region of about $8c$ side length, in which the cicada wing is placed, is discretized with high-resolution uniform grids of $0.075c$ interval to resolve the near-field flow structure. Outside the center uniform box, the grid is stretched to extend to the outer boundary with the same grid spacing used in all the six directions. Previous studies [19,21] have shown that a domain size of about $30c$ is large enough to achieve an accurate flow solution. A much larger domain here is designed to capture the flapping sound in the far-field.

For the flow solver, a uniform constant velocity U_f =2.67m/s is specified at the upstream boundary and the four lateral boundaries. A zero-gradient velocity condition is specified at the downstream boundary. A homogeneous Neumann pressure boundary is used at all the boundaries. For the acoustic solver, a non-reflective boundary condition is used at all the boundaries. The simulation is carried out with 480 flow time steps per cycle for 9 cycles. Within each flow time step, the acoustic field is solved for 30 time steps.

Due to the large domain size and small time step, storing every time frame of the acoustic field solution would require large storage capacity and longer computation time. Instead, a number of acoustic

probes are setup in the domain to continuously record the sound signal just like microphones used in the experiments. The probes are arranged on a set of spherical surfaces centered at the fixation point of the wing root. Each monitor surface has 20 grid in the latitudinal direction and 10 in the longitudinal direction with a total of 182 probe points. For example, Figure 3 shows the monitor spherical surface with a radius of $75c$. The acoustic signal was sampled 960 times per cycle, i.e. at a frequency of 44640Hz.

Also shown in Figure 3 are the planes and positions relative to the wing that are used to describe the spatial pattern of the flapping sound in the content below. The Up-Down-Left-Right plane (y-z plane) is referred to as the coronal plane without strictly pertaining to the anatomic meaning.

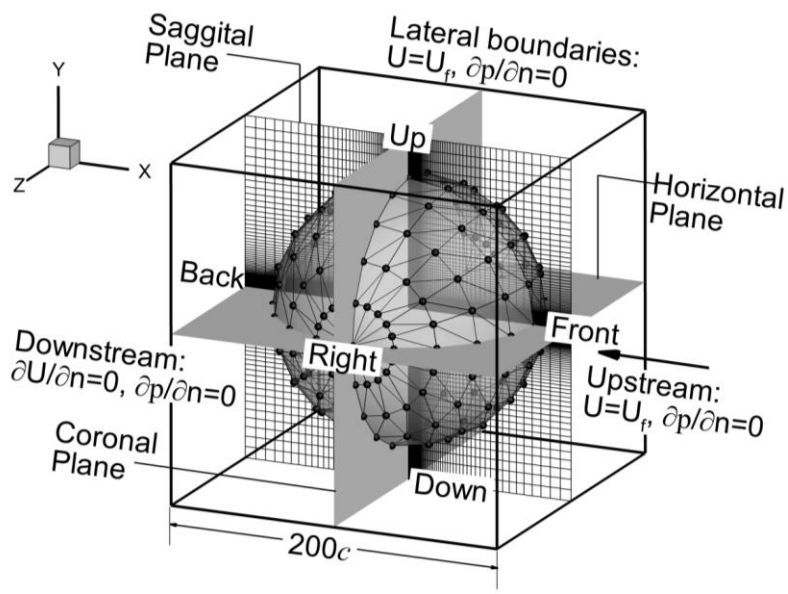

Figure 3. The computational doamin, boundary conditions, acoustic probe (black dots) setup and the reference planes and positions.

Results and discussions

For both wing models, the simulation was run for a total of 9 cycles. The acoustic pressure signals recorded at the probes for the last 6 cycles are processed with fast Fourier transform (FFT) to get the frequency composition. The amplitude of each frequency component (harmonic) is then converted into sound pressure level (SPL) with the reference pressure p_{ref} =2.0e-5 Pa.

3D radiation pattern

Figure 4 shows the contour of the amplitude (SPL in dB) of wing-beat frequency harmonic (f) for the rigid wing model at different spherical surfaces. Note that different contour levels are used in the figures

in order to clearly show the radiation pattern. A clear dipole-like radiation pattern is observed at about *r=10c* and it remains the same further from the wing. Because the near-field sound is highly influenced by the near-field flow structure **that consists of complex vortices shed by the wing**, no clear pattern was observed at *r=2c* and *r=5c*. Such sound, resulted from the fluctuating movements of the airflow rather than periodic air vibrations, is often called the pseudo-sound and it dissipates much faster than the flight sound [3] [22]. This explains why the radiation pattern becomes clear as it gets further from the wing: the pseudo-sound gets dissipated while the harmonic series remain relatively strong. As is observed by Sueur et al. [3], the pseudo-sound may [3] or may not [23] be captured in experiments depending on the relative distances of the recording to the insects. For the following of the paper, the analysis will focus on the spherical surface of *r=75c*.

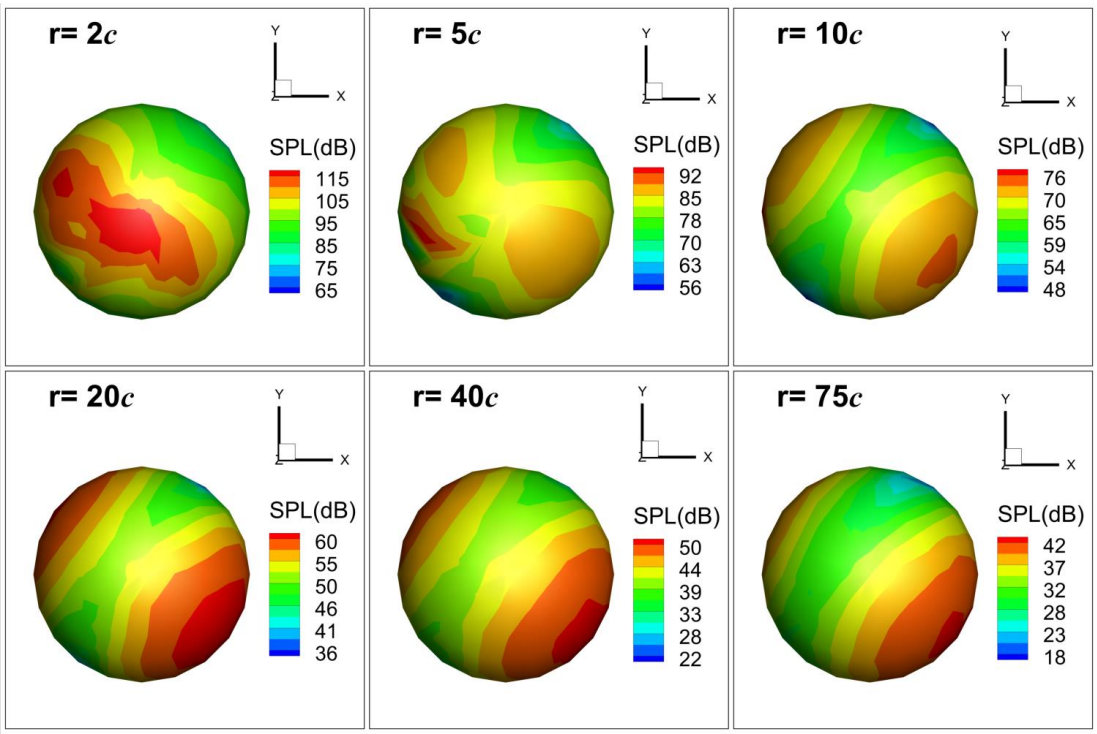

Figure 4. SPL (dB) distribution of wing-beat frequency (f) for the rigid wing model at different spherical surfaces.

Figure 5 shows the SPL (dB) distribution of the the first harmonic (f) and second harmonic ($2f$) for the rigid wing at *r=75c* from the right view and the view perpendicular to the stroke plane. Both harmonics show a dipole-like pattern, but the direction of the dipole axis is different. From the right view, the dipole axis of f is perfectly aligned with the mean stroke plane, whereas $2f$ has its peak value at the left

and right sides of the wing. From the view perpendicular to the mean stroke plane, the dipole axis of *f* is not parallel to the sagittal plane but rather rotates slightly clockwise and is almost perpendicular to the the internal bisector of the angle Φ. Such alignment isn't observed for *2f*, however. Besides, the two harmonics have comparable peak amplitudes, but the peak-valley difference is much larger for *f*.

Figure 6 shows the SPL (dB) distribution of *f* and *2f* for the flexible wing model at *r=75c* from the right view and the view perpendicular to the stroke plane. It can be seen that these two harmonics are still directional, but the directions have changed. From the right view, the dipole axis of *f* is no longer aligned with the stroke plane. Instead, it rotates toward the vertical axis. For *2f*, while the peak amplitude is still present on the left side of the wing, it's not detected on the right side. In the mean time, a relatively high amplitude of *2f* is detected right above the stroke plane (circle-marked position in Figure 5 and 6) where relatively low amplitude is detected for the rigid wing.

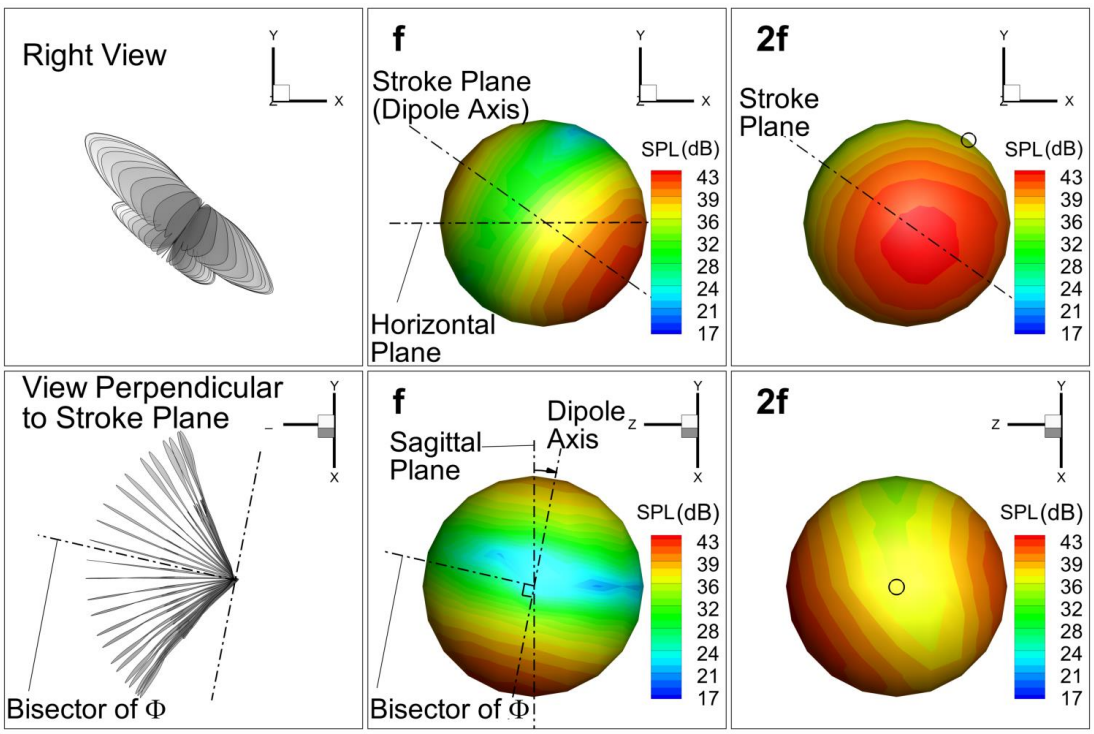

Figure 5. SPL (dB) distribution of the the first harmonic (f) and the second harmonic ($2f$) for the rigid wing model at $r = 75c$. Top row: right view. Bottom row: view perpendicular to the mean stroke plane.

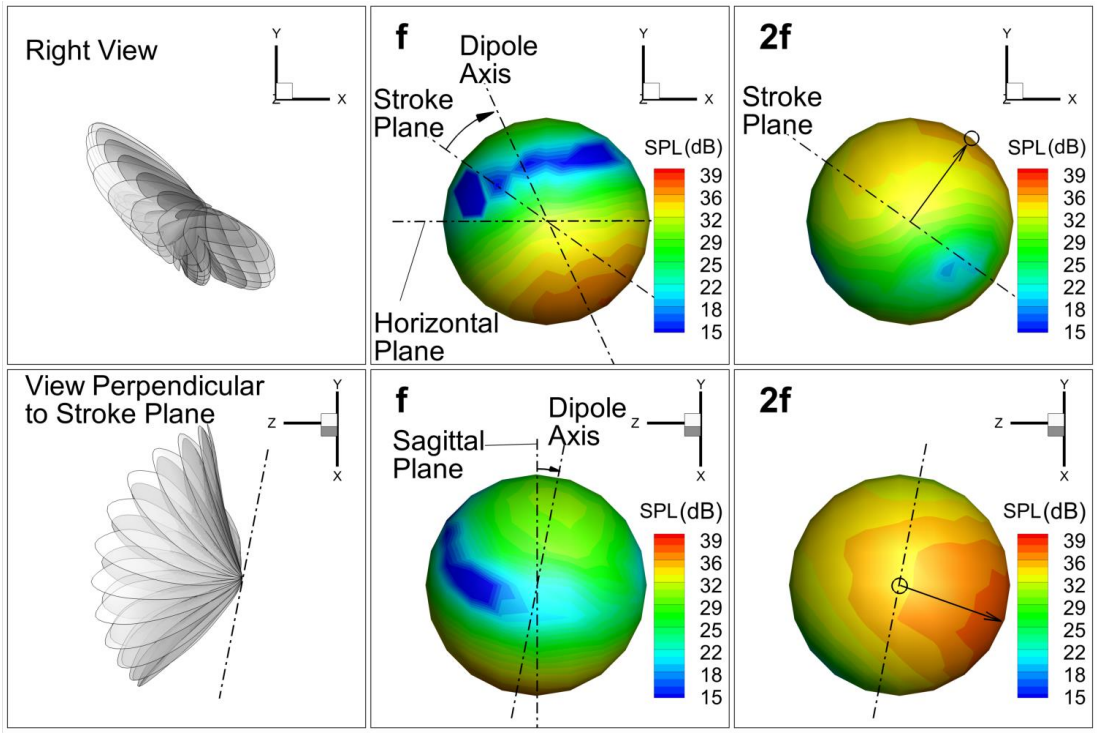

Figure 6. SPL (dB) distribution of the the first harmonic (f) and the second harmonic ($2f$) for the flexible wing model at $r = 75c$. Top row: right view. Bottom row: view perpendicular to the mean stroke plane.

Radiation in reference planes

With the 3D contour shown above, polar plots of the sound amplitude variation around the wing can be readily extracted in planes of interest. Figure 7 shows the polar plot of *f* and *2f* in the horizontal plane for the two wing models. For the rigid wing, *f* is dipole-like and *2f* is more monopole-like with a lower value at the back side. Although a dipole-like pattern is observed in 3D for *2f* in Figure 5, because the peak-valley difference is much smaller compared to that of *f*, its shape becomes more monopole-like when the same SPL scale is used. It is also found that *2f* dominates the sound spectrum at the right and left sides while *f* and *2f* have comparable amplitudes at the front and back. For the flexible wing, even though *f* is a dipole in 3D, it's not reflected in the horizontal plane, mainly because the dipole axis has rotated toward the vertical axis. *2f* only dominates the left side because right-side SPL has reduced. Sueur et al. [3] have experimentally investigated the radiation pattern around a tethered fly in the horizontal plane. Their results were similar to our rigid wing model that f was dipole-like and $2f$ was more monopole-like and $2f$ dominated the left and right sides. Difference was also noticed that, in the

experiments, f dominated the front and back, while, in our model, *f* and *2f* have comparable amplitude at the front and back. A couple of factors could contribute to why the rigid wing is closer to the experiment results. One is that since the wings of the fly are much smaller compared to the cicada wing, they might be less flexible and behave more like rigid wings, in which case as long as the mean stroke plane is not vertical, a dipole pattern would be detected in the horizontal plane. The other is that the flight condition of the tethered fly in the experiment was difficult to determine. It could be hovering flight where the mean stroke plane is parallel to the horizontal plane, in which case, a dipole pattern for *f* would also be expected for the flexible wing in the horizontal plane.

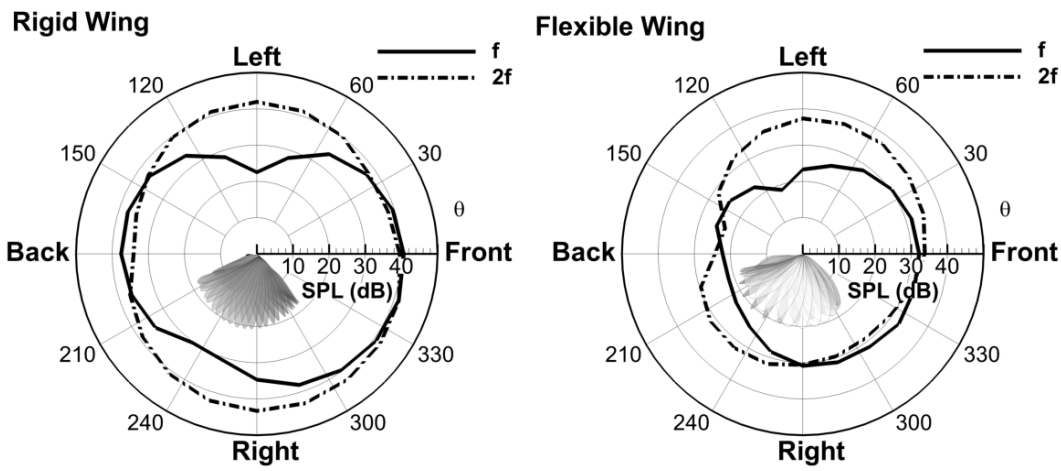

Figure 7. SPL (dB) distribution of the the harmonics (f and $2f$) for the rigid and flexible wing at $r = 75c$ in the horizontal plane.

Figure 8 and 9 show the SPL variation of *f* and *2f* of the two cases in the sagittal plane (up-down-front-back) and coronal plane (up-down-left-right), respectively. In the sagittal plane, the change of the dipole axis of *f* can be observed. Whereas the rigid wing has the dipole axis aligned with the stroke plane, the flexible wing has it rotated towards the vertical axis. Besides, the lower half of the 8-like shape is stronger than the upper half, especially in the flexible case. This "downstroke dominance" of the 8-like shape was also observed in experiments of Sueur et al. [3]. The coronal plane plots reflect that the angle between the dipole axis of *f* and the sagittal plane doesn't change from the rigid model to the flexible. And the dipole axis is roughly perpendicular to the bisector of stroke amplitude Φ, as is shown in Figure 5 and Figure 6.

The changes in *2f* from the rigid wing to the flexible wing are less clearly reflected in the 2D polar plots, mainly because the directions are no longer aligned well with the three reference planes. One noticeable change is that *2f* is significantly weaker on the right side for the flexible wing (Figure 8). The

reason might be that the wing tip trajectory for the flexible wing is different during the down- and upstroke, making the air displacement to the right side less concentrated to a single position than the rigid wing does.

The relative strength of the two frequencies is very clear for the rigid wing case: *f* dominates in the direction of the stroke plane while *2f* dominates at the left and right sides. For the flexible wing case, *f* generally dominates at the downside while the second hamonic dominates the left and up side.

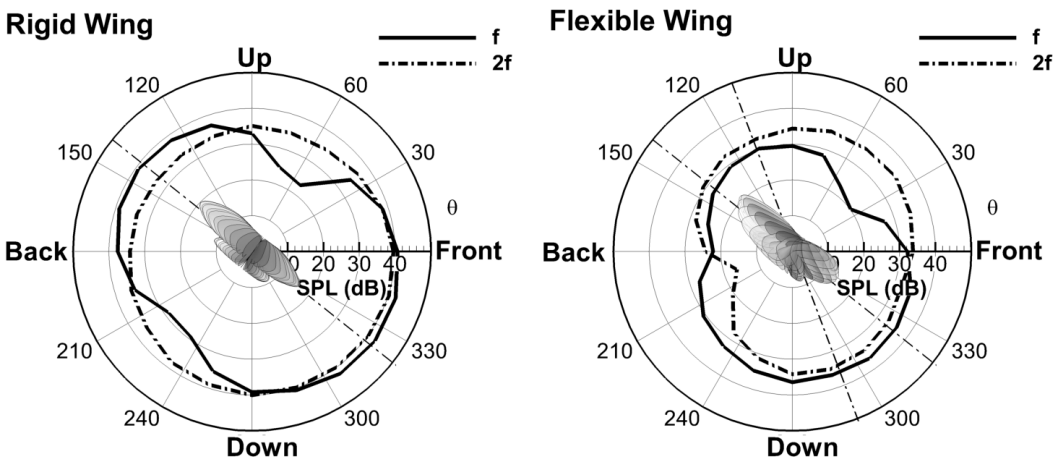

Figure 8. SPL (dB) distribution of the the harmonics (*f* and *2f*) for the rigid and flexible wing at *r=75c* in the sagittal plane.

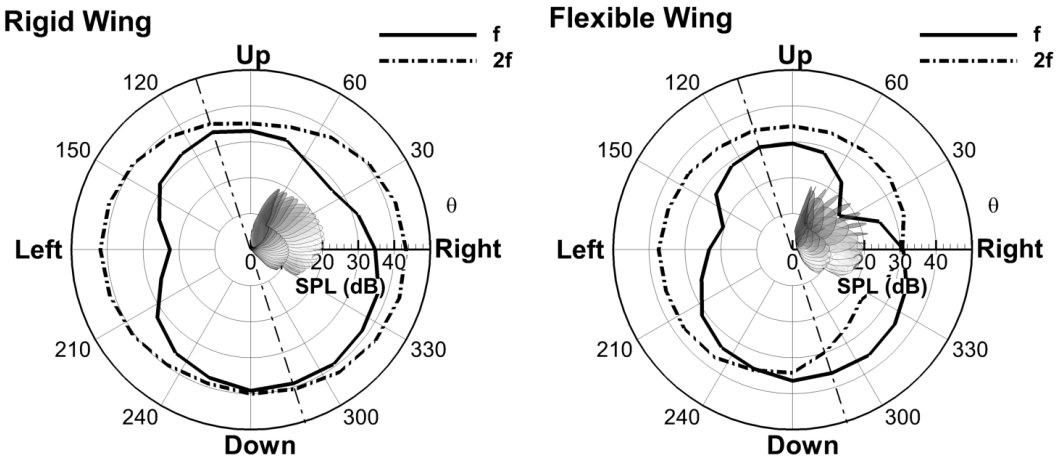

Figure 9. SPL (dB) distribution of the the harmonics (*f* and *2f*) for the rigid and flexible wing at *r=75c* in the coronal plane.

Sound generation mechanism

The directivity of flapping sound is highly related to the wing kinematics. A clear illustration of the wing-loading mechanism can be found in the work by Inada et al. [9]. The basic idea is that during a wing stroke, positive pressure is formed on the loading face due to air being displaced and negative pressure is formed on the opposite face mainly due to the leading-edge vortices. The positive and negative pressure exchange sides during the switch between the down- and upstroke. It is these pressure perturbations that propagate out and form the flapping tone. For the rigid wing case, the directivity of the harmonics is relatively easier to explain. For an observer at the two ends of the stroke plane, the pressure perturbation change signs once during one cycle, whereas for an observer at the side of the stroke plane, the pressure perturbation changes twice during one cycle. This explains the dominance of *f* in the stroke plane and dominance of *2f* at the right and left sides. For the flexible wing, it is generally the same mechanism. However, the rotation and deformation of the flexible wing could significantly affect the direction of pressure perturbation. To analyze this effect, Figure 11 shows the pressure iso-surface at the two sides of the wing at the mid-downstroke and mid-upstroke time instants for the rigid and flexible wing models, respectively. The instantaneous pressure propagation direction is roughly indicated with the double arrow. It can be seen that positive pressure is formed at the windward side of the wing and negative pressure formed at the leeward side. For both wing models, the iso-surface of the positive pressure has a more oval-like shape while the shape of the negative pressure side is more irregular due to the forming and shedding of vortices. For the rigid model where wing rotation is absent, the pressure propagation direction is consistently along the stroke plane during the entire cycle. In contrast, the flexible wing forms the dipole more towards the up-down direction at the mid-downstroke and toward the front-back direction at the mid-upstroke. This complex changing of the axis direction probably accounts for the unique pattern of *2f* shown in Figure 6. It is also observed that both models generate larger pressure loading (indicated by larger iso-surface shape) during the downstroke than during the upstroke, which might contribute to the aforementioned “downstroke dominance” phenomenon.

The changing of the pressure perturbation direction could be passively achieved through deformation due to flexibility. It could also be actively controlled through wing rotation due to torque applied at the wing base by the muscles [24], which indicates the possibility of insects voluntarily directing the flapping sound toward intended receiver, given that the same flight requirements can be achieved with different wing kinematics. One problem for insects to utilize the flapping sound is that the radiation is ineffectual [25,26], since the length of the source is generally much smaller than the wave length of the flapping sound. However, this could be possibly solved by the auditory enhancement on the receiver side [5].

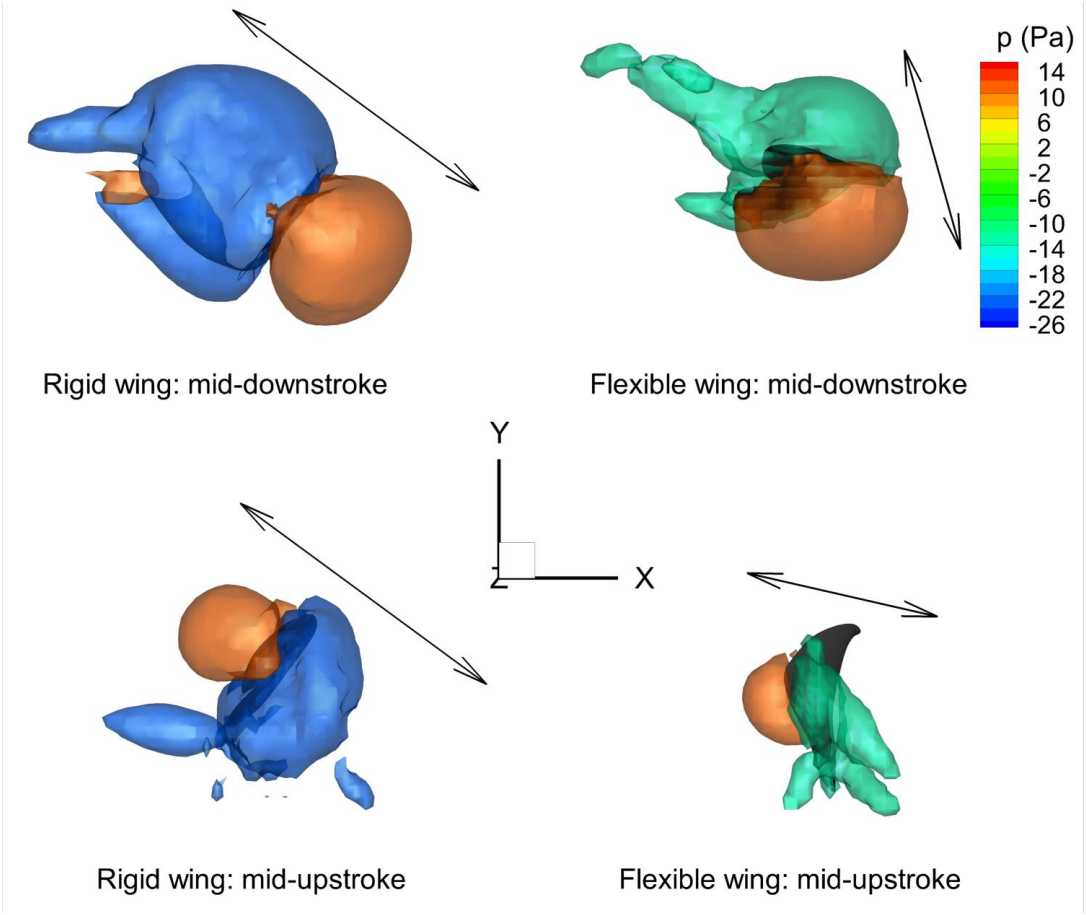

Figure 10. Pressure iso-surface at the two sides of the wing. The arrow in each plot shows roughly the pressure perturbation direction at the time instant.

The change of pressure perturbation direction is also reflected in the wing forces. The force coefficients shown in Figure 11 are calculated using

$$C_i = \frac{2F_i}{\rho U^2 A}, i = x, y, z \qquad (3)$$

where the reference velocity U is the maximum wing tip velocity and A is the area of the wing. For both wing models, while both C_x and C_y form one sinusoidal wave in one cycle, C_z forms two. It is because the pressure perturbation direction switches signs once in the stroke plane and twice in the left-right direction. It also explains the dominance of f near the two ends of the stroke plane and dominance of $2f$ at the left and right sides, as observed in Figure 7 and Figure 9. Significant differences between the two models are also observed. For the rigid wing, C_x (front-back direction) and C_y (up-down direction) are of comparable magnitude but opposite direction during the down- and upstroke, leading to a net force vector aligned with the stroke plane. The flexible wing has significantly smaller C_x, but comparable C_y during the downstroke. As result, the resultant force is more toward the vertical axis. C_y is very samll during the

upstroke for the flexible wing, which leads to the severe "downstroke dominance" of f in this case, as observed in Figure 9.

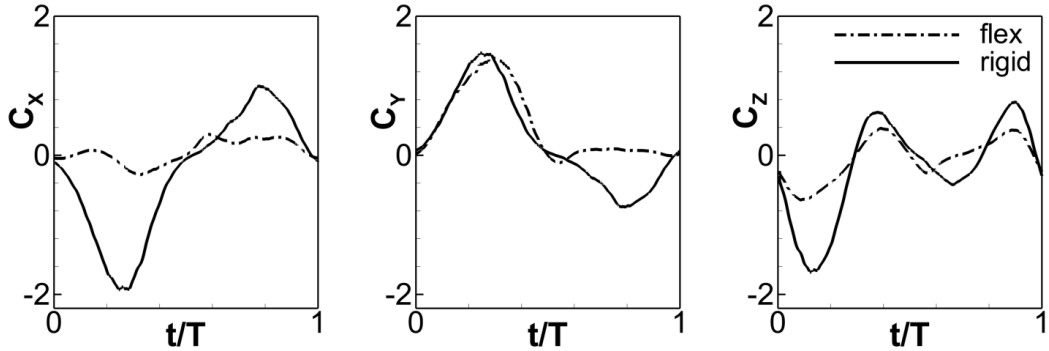

Figure 11. Force coefficients in the three directions

To further illustrate the correlation between the radiation pattern and force coefficients, FFT analysis was performed on the force coefficients to get the frequency composition of the aerodynamic forces. The force coefficient vector was first projected onto the normal direction at each probe point on the spherical surface using

$$C_N(\vec{r},t) = \{C_X(t), C_Y(t), C_Z(t)\} \cdot \frac{\vec{r}}{|\vec{r}|} \quad (4)$$

where the aerodynamic signal C_N is the normal component of the force coefficient vector at each probe point identified by the vector $\vec{r}$ that points from the center of the sphere to the probe point. The aerodynamic signal C_N at each probe point was then used as the input for the FFT. Figure 12 and 13 compare the acoustic signal pattern and aerodynamic signal pattern for the rigid wing and flexible wing, respectively. It can be observed that the acoustic signal pattern highly match the aerodynamic signal pattern for both f and $2f$ for the rigid wing model and f for the flexible wing model. The mismatch of $2f$ of the flexible wing model may be related to the dipole axis change of the pressure perturbation observed in Figure 10, which could result in complex pressure perturbation pattern in far-field. Nevertheless, the high similarity of the harmonic distribution between the acoustic signal and the aerodynamic signal consolidates the hypothesis that the flapping sound is primarily generated by wing loading. **Based on this hypothesis, the radiation pattern as well as the magnitude of the flapping sound would change with the flight speed due to the change in wing loading. As the flight speed increases, more thrust needs to be generated to offset the drag while the lift remains equal to the body weight of the flyer. Accordingly, the wing loading becomes increasingly asymmetrical between**

the down- and upstroke. Other flight condition or wing kinematics changes that lead to different wing loadings are speculated to change the radiation pattern and magnitude in a similar way. Generally, factors that have a larger impact on the wing loading would also have a larger impact on the magnitude of the flapping sound.

Besides the changes in the radiation directivity, the flexible wing is observed to have lower SPL in all the directions for both *f* and *2f*. In the contour plots shown in Figure 5 and Figure 6, the peak SPL value for the rigid model is about 4dB higher than the flexible model. And in the reference planes, the envelope of the flexible model is basically contained in the envelope of the rigid model. This implies that the flexibility of the wing is beneficial for reducing flight noise. The lower sound of the flexible model is due to the lower aerodynamic forces caused by wing deformation as seen in Figure 11.

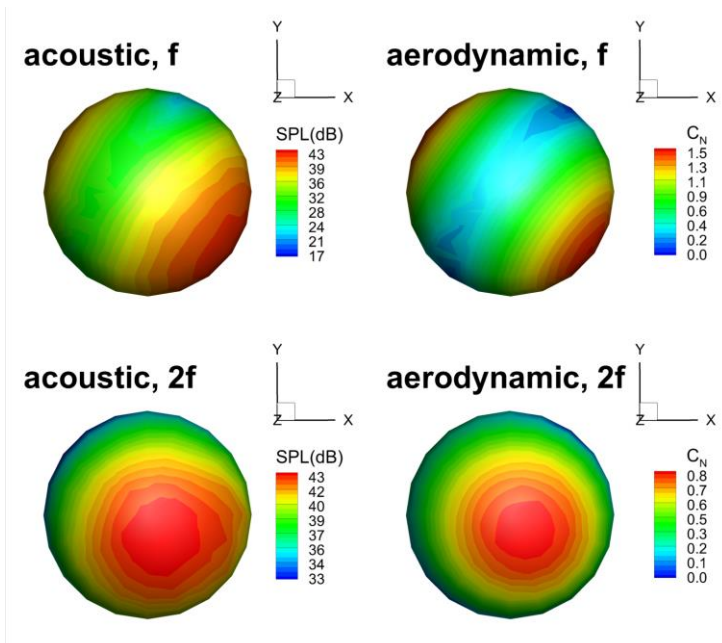

Figure 12. Comparison of acoustic signal pattern (left column) and aerodynamic signal (C_N, right column) pattern for the rigid wing model.

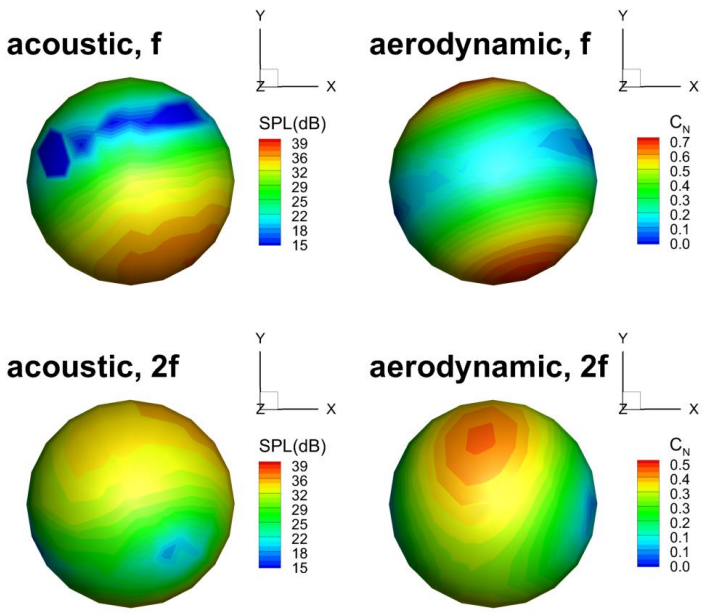

Figure 13. Comparison of acoustic signal pattern (left column) and aerodynamic signal (C_N) pattern (right column) for the flexible wing model.

CONCLUSION

The flapping sound are numerically investigated for three-dimensional (3D) models of Tibicen linnei cicada at free forward flight condition with the prescribed motion reconstructed from high-speed videos of a live flying cicada. Along with the flexible wing model, a rigid wing model that is extracted from the real motion is also simulated to investigate the effect of wing flexibility. Main findings and conclusions are listed below.

(1) The simulation results show that the flapping sound is directional; the 3D radiation pattern becomes clear at about 10 chord length from the wing and remains the same beyond.

(2) For both wing models, the dominant frequency varies round the wing. For the rigid wing model, f dominates in the direction of the stroke plane, and $2f$ dominates at the left and right sides. For the flexible wing model, f dominates the down side and $2f$ dominates the left and up sides.

(3) Both f and the $2f$ show a dipole-like pattern in 3D, but the direction of the dipole axis is different in two cases. In the rigid wing model, the dipole axis of f is perfectly align with the stroke direction while, in the flexible wing model, the axis has shifted toward the vertical direction. The axis of $2f$ for both wing models lies in the left-right direction. However, $2f$ has comparable amplitudes between

the left and right sides in the rigid wing model, while, in the flexible wing model, it shows a lower amplitude at the right side. Such radiation patterns explain the variation of sound dominance mentioned above.

(**4**) The radiation patterns of *f* and *2f* are highly associated with wing kinematics and loadings. The reason of the shift of dipole axis of *f* in the flexible wing model is that the rotation and deformation of the wing has changed the pressure perturbation direction more toward the vertical direction in the downstroke and diminished the pressure perturbation in the upstroke. This effect has also resulted in a severer "downstroke dominance" phenomenon in the flexible wing model. Furthermore, the rotation and deformation of the flexible wing has also resulted in different pressure perturbation directions in the downstroke and upstroke, which may be responsible for the change of $2f$ radiation pattern in the flexible wing case. These effects are also reflected in the force coefficients curves.

(**5**) Compared to the rigid wing motion, the flexible wing generates lower sound, which is also consistent with the wing loading signals.

Currently, only the right wing is modeled. While it's helpful for understanding the very basic component of the sound source of the flapping sound, it's unclear how the pressure perturbation from a pair of wings would interact and how the resultant acoustic field would superimpose with each other. Modelling of the whole insect would be of interest for future studies.

ACKNOWLEDGMENT

This research was supported by NSF grant CBET-1313217 and AFOSR grant FA9550-12-1-0071.

REFERENCES

[1] Sane, S. P., 2003, "The Aerodynamics of Insect Flight.," J. Exp. Biol., **206**(Pt 23), pp. 4191–4208.

[2] Wang, Z. J., 2005, "Dissecting Insect Flight," Annu. Rev. Fluid Mech., **37**(1), pp. 183–210.

[3] Sueur, J., Tuck, E. J., and Robert, D., 2005, "Sound Radiation around a Flying Fly.," J. Acoust. Soc. Am., **118**(April), pp. 530–538.

[4] Bae, Y., and Moon, Y. J., 2008, "Aerodynamic Sound Generation of Flapping Wing.," J. Acoust. Soc. Am., **124**(1), pp. 72–81.

[5] Jackson, J. C., and Robert, D., 2006, "Nonlinear Auditory Mechanism Enhances Female Sounds for Male Mosquitoes.," Proc. Natl. Acad. Sci. U. S. A., **103**(45), pp. 16734–16739.

[6] Srygley, R. B., 2007, "Evolution of the Wave: Aerodynamic and Aposematic Functions of Butterfly Wing Motion.," Proc. Biol. Sci., **274**(1612), pp. 913–917.

[7] Clark, C. J., 2016, *Vertebrate Sound Production and Acoustic Communication*.

[8] Robert, D., and Göpfert, M. C., 2002, "Acoustic Sensitivity of Fly Antennae," J. Insect Physiol.,

48(2), pp. 189–196.

[9] 2010, "Numerical Analysis of Sound Generation of Insect Flapping Wings.pdf," Theor. Appl. Mech. Japan, **57**, pp. 437–447.

[10] Young, J., Walker, S. M., Bomphrey, R. J., Taylor, G. K., and Thomas, A. L. R., 2009, "Details of Insect Wing Design and Deformation Enhance Aerodynamic Function and Flight Efficiency.," Science, **325**(5947), pp. 1549–52.

[11] Ren, Y., and Dong, H., 2016, "Low-Dimensional Modeling and Aerodynamics of Flexible Wings in Flapping Flight," *34th AIAA Applied Aerodynamics Conference*, p. 4168.

[12] Eldredge, J. D., Toomey, J., and Medina, A., 2010, "On the Roles of Chord-Wise Flexibility in a Flapping Wing with Hovering Kinematics," J. Fluid Mech., **659**, pp. 94–115.

[13] Heathcote, S., Wang, Z., and Gursul, I., 2008, "Effect of Spanwise Flexibility on Flapping Wing Propulsion," J. Fluids Struct., **24**(2), pp. 183–199.

[14] Zhao, L., Huang, Q., Deng, X., and Sane, S. P., 2010, "Aerodynamic Effects of Flexibility in Flapping Wings.," J. R. Soc. Interface, **7**(44), pp. 485–97.

[15] Mittal, R., Dong, H., Bozkurttas, M., Najjar, F. M., Vargas, A., and von Loebbecke, A., 2008, "A Versatile Sharp Interface Immersed Boundary Method for Incompressible Flows with Complex Boundaries," J. Comput. Phys., **227**(10), pp. 4825–4852.

[16] Zheng, X., Xue, Q., Mittal, R., and Beilamowicz, S., 2010, "A Coupled Sharp-Interface Immersed Boundary-Finite-Element Method for Flow-Structure Interaction with Application to Human Phonation," J. Biomech. Eng., **132**(11), p. 111003.

[17] Seo, J. H., and Moon, Y. J., 2006, "Linearized Perturbed Compressible Equations for Low Mach Number Aeroacoustics," J. Comput. Phys., **218**(2), pp. 702–719.

[18] Seo, J. H., and Mittal, R., 2011, "A High-Order Immersed Boundary Method for Acoustic Wave Scattering and Low-Mach Number Flow-Induced Sound in Complex Geometries," J. Comput. Phys., **230**(4), pp. 1000–1019.

[19] Liu, G., Dong, H., and Li, C., 2016, "Vortex Dynamics and New Lift Enhancement Mechanism of Wing–body Interaction in Insect Forward Flight," J. Fluid Mech., **795**, pp. 634–651.

[20] Koehler, C., Liang, Z., Gaston, Z., Wan, H., and Dong, H., 2012, "3D Reconstruction and Analysis of Wing Deformation in Free-Flying Dragonflies," J. Exp. Biol., **215**(17), pp. 3018–3027.

[21] Wan, H., Dong, H., and Gai, K., 2014, "Computational Investigation of Cicada Aerodynamics in Forward Flight," J. R. Soc. Interface, **12**(102), pp. 20141116–20141116.

[22] Lighthill, M. J., 1962, "The Bakerian Lecture, 1961. Sound Generated Aerodynamically," *Proceedings of the Royal Society of London A: Mathematical, Physical and Engineering Sciences*, pp. 147–182.

[23] Bennet-Clark, H. C., and Ewing, A. W., 1968, "The Wing Mechanism Involved in the Courtship of Drosophila," J. Exp. Biol., **49**(1), pp. 117–128.

[24] Dudley, R., 2002, *The Biomechanics of Insect Flight: Form, Function, Evolution*, Princeton University Press.

[25] Fletcher, N. H., 1992, *Acoustic Systems in Biology*, Oxford University Press.

[26] Bennet-Clark, H. C., 1998, "Size and Scale Effects as Constraints in Insect Sound Communication," Philos. Trans. R. Soc. B Biol. Sci., **353**(1367), pp. 407–419.